Baltic Astronomy, vol. 8, 203–232, 1999.

THE STAR FORMATION HISTORY OF THE MILKY WAY: METHODOLOGY AND IMPLICATIONS FOR GAIA

G. Gilmore

Institute of Astronomy, Cambridge University, Madingley Road, Cambridge CB3 0HA, England

Received April 20, 1999.

Abstract. Objective determination of a star formation history from a colour-magnitude diagram, independently of assumed parametric descriptions, is a requirement if *Gaia* is to determine the evolutionary history of the Galaxy. We introduce a new method for solving maximum likelihood problems through variational calculus, and apply it to the case of recovering an unknown star formation history, $SFR(t)$, from a resulting HR diagram. This approach allows a totally non-parametric solution which has the advantage of requiring no initial assumptions on the $SFR(t)$.

Key words: Galaxy: stellar content, star formation history, evolution – stars: HR diagram, fundamental parameters – orbiting observatories: Gaia

1. INTRODUCTION

A primary scientific requirement of the *Gaia* mission is determination of the star formation histories, as described by the temporal evolution of the star formation rate, $SFR(t)$, and the cumulative numbers of stars formed, of the bulge, inner disk, solar neighbourhood, outer disk and halo of the Milky Way. In practise, uncertainties in the theories of stellar formation and evolution, as well as degeneracy in a stars' observational parameters between age and metallicity, not to mention observational errors and unknown distance and reddening corrections, make inferring $SFR(t)$ for mixed stellar populations difficult. Even assuming a known stellar initial

mass function (IMF) and metallicity, a given set of isochrones and no distance or reddening uncertainties, recovering the $SFR(t)$ which gave rise to a given HR diagram is not trivial.

The increasing application of HST studies which resolve the stellar populations of nearby systems has initiated quantitative investigation of the $SFR(t)$ in these systems through comparison of the observed HR diagram with synthetic ones e.g. Chiosi et al. (1989), Aparicio et al. (1990) and Mould et al. (1997) using Magellanic and local clusters, and Mighell & Butcher (1992), Smecker-Hane et al. (1994), Tolstoy (1995), Aparicio & Gallart (1995) and Mighell (1997) using dSph companions to the Milky Way. The framework within which this problem is generally faced is to construct a statistical estimator of how closely a synthetic HR diagram constructed from an assumed $SFR(t)$ resembles the observed one, and then to select the $SFR(t)$, from amongst a set of plausible ones, which maximizes the value of this estimator (e.g. Tolstoy & Saha 1996). The most rigorous estimator is probably the likelihood, as defined through Bayes's theorem. In practice this states that one should look for the model which maximizes the probability of the observed data set having arisen from it. In comparing two or more candidate models through the likelihood one takes into account the position of each star in the observed HR diagram, there being no necessity to smooth the data into a continuous distribution, or to include only specific features of the HR diagram, such that all the available information contributes to the comparison. The robustness of the approach is undermined by the degree of subjectivity associated with defining the set of plausible models one is going to consider. Further, as none of the statistical estimators has an absolute normalization, in the end one is left with that model, of the ones one started by proposing, which best reproduces the data, which might not necessarily be a "good" approximation to the true $SFR(t)$. The likelihood of the data having arisen from a particular model can only be calculated if one has the data, the errors, and the particular model fully specified. This last condition has led to the almost exclusive use of parametric $SFR(t)$'s.

However, in real stellar systems, one expects a complex $SFR(t)$, where the aim of a particular parameterization is to reject a particular astrophysical model and favour another. If it is the precise form of the $SFR(t)$ which serves as a constraint on a theory (e.g. a collection of randomly located bursts as fragments accrete or a more uniform function as gas cools, for the build up of the Galaxy), one

must consider the most general $SFR(t)$. The less one assumes *a priori* about the $SFR(t)$ one is solving for, the more objective the inference will be.

A first attempt at solving for $SFR(t)$ non parametrically is to break the star formation history into a series of bursts, and to solve for the amplitude of each one e.g. Dolphin (1997). Other variants of this approach are possible, for example Hurley-Keller et al. (1998) who parameterize the $SFR(t)$ of the Carina dwarf as consisting of 3 bursts, and solve for the positions, durations and amplitudes of each. In principle, as the number of bursts considered tends to infinity, the full $SFR(t)$ is recovered. The difficulty in increasing the number of bursts considerably lies in that each extra burst increases the *dimension* of the parameter space by at least one. As the likelihood hyper-surface will in general be quite complex, the only reliable way of finding the absolute maximum is to evaluate the likelihood function over the entire parameter space. This last procedure is clearly not a practical approach, as calculating the likelihood of a complete set of thousands of observed stars for even one single model is a lengthy procedure, let alone throughout a 100 or more dimensional space.

Further, methods which consider a large parameter space often do not use a full likelihood analysis, but simpler statistical estimators such as luminosity functions (Aparicio & Gallart 1995, Mighell 1997). In this last approach the HR diagram is divided into cells and the numbers of stars in each used as independent variables to construct a statistical estimator. The resulting statistic is not strictly rigorous as the numbers of stars in different cells are in fact correlated through the underlying IMF and $SFR(t)$. Presently, methods of comparing simulated HR diagrams with observations can be classified according to the statistical criterion used in the comparison. A few examples of the variety in these categories are Tolstoy (1995) and Mould et al. (1997) who use full maximum likelihood statistics, Dolphin (1997) and Ng (1998) who use chi-squared statistics, and Aparicio et al. (1997) and Hurley-Keller et al. (1998) who break the HR diagrams into luminosity functions before constructing the statistical estimator.

Since *Gaia* and the Milky Way evaluation require a more general approach, we (Hernandez, Valls-Gabaud & Gilmore 1999 MNRAS in press; Hernandez, Gilmore & Valls-Gabaud 1999, MNRAS submitted) developed a variational calculus method of solving directly for the maximum likelihood $SFR(t)$, which does not require any

assumptions on the function one is trying to recover, or to evaluate the likelihood of any of the $SFR(t)$'s being considered (all continuous functions of time). We construct an integro-differential equation which is iterated to find a $SFR(t)$ which yields a vanishing first variation for the likelihood. At each iteration the $SFR(t)$ is solved with an arbitrary time resolution. Conveniently, computation times scale only linearly with this time resolution. This allows a very fine reconstruction of the $SFR(t)$, which would be prohibitively expensive in a parametric decomposition of the $SFR(t)$.

Full details of the model, the extensive tests and calibrations, and its application to new HST data for the galactic dSph satellites, are presented in the references noted (Hernandez et al. 1999a, 1999b). In this note I summarize the method and its validity. I then simulate *Gaia* observations of an old metal-poor stellar population, a young metal rich population, and a mixed population. These simulations show that *Gaia* data can indeed meet the scientific goal required, quantify the metallicity accuracy needed, and quantify the photometric precision required by *Gaia* at faint magnitudes.

2. DERIVING STAR FORMATION HISTORIES

Our goal is to recover the star formation history which gave rise to an observed population of stars, described by $SFR(t)$, the star formation rate as a function of time. As we want our method to be of a very general applicability, we shall assume absolutely nothing about the $SFR(t)$ we are trying to recover, beyond that it be a continuous function of time. It is important not to impose any *a priori* parameterization on $SFR(t)$, since it is precisely the form of this function that we are trying to recover from the data: $SFR(t)$ will be fixed entirely by the data. One obvious constraint will be the total number of stars produced, which furnishes a normalization condition on $SFR(t)$, over the range of masses over which stars can be observed. Obtaining the faint end slope of the initial mass function is an entirely different problem which we shall not address. Here we will be concerned only with that fraction of the total star formation which produced stars still readily visible today. It is this that we are calling the $SFR(t)$. We note that this requires an accurate determination of the local *Gaia* completeness limit, but does not imply that this completeness limit have a value near unity.

The final observed HR diagrams as a function of place are the result of the star formation histories in those places, later dynamical

evolution, and also of the relevant initial mass function, the metallicity and the stellar evolutionary processes. As we see later, it is essential that the IMF near the turnoff, and the star by star metallicity, be independently known. It is this requirement which is the primary science case for *Gaia* to determine stellar metallicity, and which constrains the requisite photometric performance. [Note that there are other astrophysical systems for which this essentially holds, and for which only the star formation history is poorly known. Examples of such systems are some of the dwarf spheroidal companions to our Galaxy, whose star formation histories we have derived.]

Further, we are only interested in the stars which end up in the observations at the distance of the galactic center, and the stellar edge of the disk. This determines the mass regime over which the initial mass function needs to be well established. Theoretical studies of stellar isochrones have advanced significantly over the last decade, and now there seems to be little uncertainty in the physical properties of stars over the mass range 0.6–3 solar masses, during all but the shortest lived periods. Here we are using the latest Padova isochrones (Fagotto et al. 1994, Girardi et al. 1996), including most stages of stellar evolution up to the RGB phase. Our detailed inferences will depend on the precise details of the isochrones we use. Our aim here is not to insist upon any particular age calibration, but basically to prove the method. Any and all isochrones can be used.

2.1. The method

Having a fixed set of observations $A = (A_1, ..., A_n)$, which we are assuming resulted from a model which belongs to a certain known set of models $B = B_1, ...$ we want to find the model which has the highest probability of resulting in the observed data set, A. That is, we wish to identify the model which maximizes $P(AB_i)$, the joint probability of A occurring for a given model B_i. From the definition of conditional probabilities,

$$P(AB_i) = P(A|B_i) \cdot P(B_i) = P(B_i|A) \cdot P(A) \qquad (1)$$

where $P(A|B_i)$ is the conditional probability of observing A given a fixed model B_i occurred, $P(B_i|A)$ is the conditional probability of model B_i given the observed data A, and $P(A), P(B_i)$ are the independent probabilities of A and B_i, respectively. Further, if the B_is are exclusive and exhaustive,

$$P(A) = \int_i P(A|B_i) \cdot P(B_i) = 1/C \tag{2}$$

where C is a constant, so that equation (1) becomes:

$$P(B_i|A) = C \cdot P(A|B_i) \cdot P(B_i) \tag{3}$$

which is Bayes' theorem. $P(B_i)$ is called the *prior* distribution, and defines what is known about model B_i without any knowledge of the data. As we want to maximize the relevance of the data in our inference, we can take the hypothesis of equal prior probabilities, finding the maximum likelihood model under this assumption is hence simplified to finding the model B_i for which $P(A|B_i)$ is maximized. Our set of models from which the optimum $SFR(t)$ is to be chosen includes all continuous, twice differentiable functions of time such that the total number of stars formed does not conflict with the observed HR diagram.

In order to find the $SFR(t)$ which maximizes the probability of the observed HR diagram resulting from it, we first have to introduce a statistical model to calculate the probability of the data resulting from a given $SFR(t)$. Take one particular star, having an observed luminosity and colour, l_i, c_i, and an intrinsic luminosity and colour L_i, C_i, which will usually differ due to observational errors, where the index $1 < i < n$ distinguishes between the n observed stars making up the HR diagram. The probability of this observed point being a star belonging to a particular isochrone $C(L; t_j)$, i.e., being part of the stars formed by $SFR(t_j)$ will be given by:

$$P_i(t_j) = SFR(t_j) \frac{\rho(L_i; t_j)}{\sqrt{2\pi}\sigma(l_i)} \exp\left(\frac{-[C(L_i; t_j) - c_i]^2}{2\sigma^2(l_i)}\right). \tag{4}$$

In Eq. (4) $\sigma(l_i)$ denotes the observational error in the measurement of the colour of the ith observed star, which is a function of the luminosity of this star, and which we are assuming follows a Gaussian distribution. In real data, the errors in the luminosity are much smaller than in the colour determination, which comes from subtracting two observed quantities. For simplicity, we only consider errors in the colour, which increase with decreasing luminosity, in a way determined by the particular observation. In this case $L_i = l_i$ which we adopt throughout, the generalization to an error ellipsoid being trivial. $C(L_i; t_j)$ is the colour the observed star having luminosity l_i

would have if it had actually formed at $t = t_j$. $\rho(L_i; t_j)$ is the density of stars along the isochrone $C(L; t_j)$ around the luminosity of the observed star, l_i, for an isochrone containing a unit total mass of stars. Therefore, for stars in their main sequence phase, $\rho(L; t_j)$ is actually the initial mass function expressed in terms of the luminosity of the stars. Further along the isochrone it contains the initial mass function convolved with the appropriate evolutionary track. Finally, $SFR(t_j)$ indicates the total mass of stars contained in the isochrone in question, and is the only quantity in Eq. (4) which we ignore, given an observational HR diagram, an initial mass function and a continuous set of isochrones.

The probability of the observed point l_i, c_i being the result of a full given $SFR(t)$ will therefore be:

$$P_i\big(SFR(t)\big) = \int_{t_0}^{t_1} SFR(t) G_i(t) dt \tag{5}$$

where

$$G_i(t) = \frac{\rho(L_i; t)}{\sqrt{2\pi}\sigma(l_i)} exp\left(\frac{-[C(L_i; t) - c_i]^2}{2\sigma^2(l_i)}\right)$$

and where t_0 and t_1 are a maximum and a minimum time needed to be considered, for example 0 and 15 Gyr. We shall refer to $G_i(t)$ as the likelihood matrix. At this point we introduce the hypothesis that the n different observed points making up the total HR diagram are independent events, to construct:

$$\mathcal{L} = \prod_{i=1}^{n} \left(\int_{t_0}^{t_1} SFR(t) G_i(t) dt\right) \tag{6}$$

which is the probability that the full observed HR diagram resulted from a given $SFR(t)$. This first part is essentially well known, and we have presented it as it was laid out in Tolstoy & Saha (1996), who use Eq. (6) to compare between different set proposed $SFR(t)'s$.

The remainder of the development is entirely new. We shall use Eq. (6) to construct the Euler equation of the problem, and hence obtain an integro-differential equation directly for the maximum likelihood $SFR(t)$, about which we shall assume nothing *a priori*. It is the functional $\mathcal{L}(SFR(t))$ which we want to maximize with respect to $SFR(t)$ to find the maximum likelihood star formation history.

The condition that $\mathcal{L}(SFR)$ has an extremal can be written as

$$\delta\mathcal{L}(SFR) = 0,$$

and the techniques of variational calculus brought to bear on the problem. Firstly, we develop the product over i using the chain rule for the variational derivative, and divide the resulting sum by $\mathcal{L}$ to obtain:

$$\sum_{i=1}^{n} \left(\frac{\delta \int_{t_0}^{t_1} SFR(t) G_i(t) dt}{\int_{t_0}^{t_1} SFR(t) G_i(t) dt} \right) = 0. \tag{7}$$

In order to construct an integro-differential equation for $SFR(t)$ we introduce the new variable $Y(t)$ defined as:

$$Y(t) = \int \sqrt{SFR(t)} dt \Longrightarrow SFR(t) = \left(\frac{dY(t)}{dt} \right)^2$$

Introducing the above expression into Eq. (7) and developing the Euler equation yields,

$$\frac{d^2Y(t)}{dt^2} \sum_{i=1}^{n} \left(\frac{G_i(t)}{I(i)} \right) = -\frac{dY(t)}{dt} \sum_{i=1}^{n} \left(\frac{dG_i/dt}{I(i)} \right) \tag{8}$$

where

$$I(i) = \int_{t_0}^{t_1} SFR(t) G_i(t) dt.$$

We have thus constructed an integro-differential equation whose solution yields a $SFR(t)$ for which the likelihood has a vanishing first variation. This in effect has transformed the problem from one of searching for a function which maximizes a product of integrals (Eq. 6) to one of solving an integro-differential equation (Eq. 8). Solving Eq. (8) will be the main problem, as this would yield the required star formation history directly, without having to calculate $\mathcal{L}$ explicitly over the whole space containing all the possible $SFR(t)s$.

One may now implement an iterative scheme for solving Eq. (8), the details of which are given in Hernandez, Vall-Gabaud & Gilmore (1999). Given the complexity of the isochrones, the initial mass function and the unknown star formation histories we are trying to recover, it is not possible to prove convergence analytically for the implemented iterative method. Hernandez et al. show that the method works remarkably well for a wide range of synthetic HR diagrams produced from known $SFR(t)$'s, independent of the initialization used.

3. TESTING THE METHOD: A SUMMARY

To illustrate the validity of the method, we present here a subset of the simulation results of Hernandez et al., where further details may be found. The method used here is to create an artificial colour-magnitude diagram from a set of adopted star formation histories, and then to apply the method above to deduce a star formation history from the CMD. The true simulation input and the derived output are compared.

Important general features of these simulations include the age resolution, choice of isochrones, and adopted IMF. To produce a realistic HR diagram from a proposed $SFR(t)$ requires firstly a method of obtaining the colour and luminosity of a star of a given mass and age. Interpolating between isochrones is a risky procedure which can imprint spurious structure in the inference procedure, given the almost discontinuous way that stars' properties vary across critical points along the isochrones, and how these critical points vary with time and metallicity.

To avoid this we use the latest Padova (Fagotto et al. 1994, Girardi et al. 1996) full stellar tracks, calculated at fine variable time intervals, and a careful interpolating method which uses only stars at constant evolutionary phases to construct an isochrone library. We calculate 100 isochrones containing 1000 uniformly spaced masses each, with a linear spacing between 0.1 and 15 Gyr, which determines the time resolution with which we implement the method to be 150 Myr. An arbitrary time resolution can be achieved using a finer isochrone grid, which only increases the calculation times linearly with the number of intervals. Unless otherwise stated, we assume a metallicity of $[Fe/H]_{\odot} = -1.7$ for the tests of the method. Although in comparison with real data one uses colours and magnitudes, trying to make these first tests as clean as possible, we perform them on the theoretical HR diagram, in terms only of temperature (T) and luminosity (L). Units throughout are $L_{\odot}$, degrees K, t Gyr and $M_{\odot}$/Gyr.

Having fixed the isochrones, we now need to specify the manner in which the density of stars will vary along these isochrones, i.e. an IMF. We use the IMF derived by Kroupa et al. (1993), where a single fit to this function is seen to hold for stars towards both galactic poles, and for all stars in the solar neighborhood. In analyzing the stellar distribution towards the galactic poles, a wide range of metallicities and ages is sampled, and care was taken to account for all

the effects this introduces, including the changing mass-luminosity relation at different ages and metallicities, completeness effects as a function of luminosity and distance, and the contribution of binaries. At this point we shall assume their result to be of universal validity, and use their fit:

$$\rho(m) \propto \begin{cases} m^{-1.3} & 0.08M_\odot < m \leq 0.5M_\odot \\ m^{-2.2} & 0.50M_\odot < m \leq 1.0M_\odot \\ m^{-2.7} & 1.00M_\odot < m \end{cases} \quad (9)$$

We normalize this relation such that a unit total mass is contained upwards of $0.08M_\odot$, although only stars in the mass range $0.6-3M_\odot$ can end up in the HR diagram. We can now choose a $SFR(t)$, and use the IMF of Eq. (9) to populate our isochrones and create a synthetic HR diagram, after including "observational" errors, assumed as Gaussian on $\log T$). The dispersion is assumed to depend only on L, and as an illustrative example we will use:

$$\sigma(L) = \frac{0.035}{[log(L)+1]^{1.5}}. \quad (10)$$

3.1. A simple 2-burst example

As a first test we use a $SFR(t)$ consisting of two Gaussian bursts at different epochs, of different amplitudes and total masses. This $SFR(t)$ is shown by the dashed line in the right panel of Fig. 1, where the time axis shows the age of the corresponding stellar populations. The left panel of Fig. (1) shows the resulting HR diagram which contains a total of 3819 stars. To ensure a realistic error structure the shape of Eq. (10) was obtained from a fit to the errors of the HST observations of dSph galaxies of Unavane and Gilmore (private communication). The amplitude of this error is representative of what is seen in current HST observations, corresponding to a few percent photometric errors in broad-band colours at the turnoff. It is comparable to *Gaia* data for the galactic bulge. From the synthetic HR diagram the general features of the input $SFR(t)$ can be seen, in that two basic populations are evident. Obtaining the precise duration and location of these two bursts requires more work, and the detailed shape of each is quite hard to recover.

From the position of every one of the 1324 simulated stars with $\log L) > 0$ on Fig. (1) (see below) we construct the matrix $G_i(t)$,

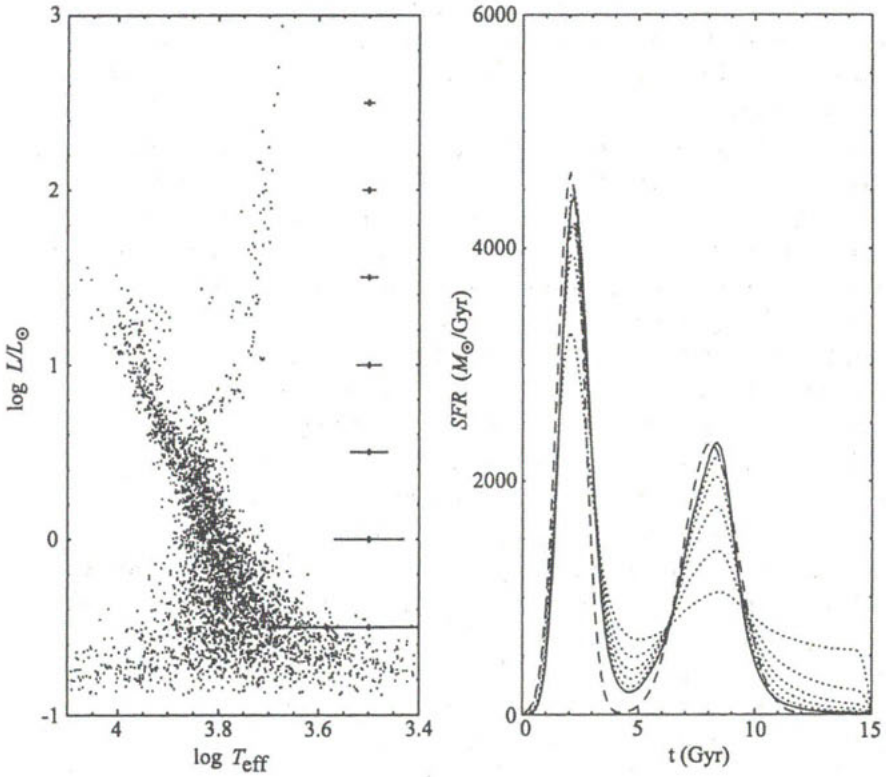

Fig. 1. Left: synthetic HR diagram resulting from the first input $SFR(t)$. The length of the bars to the right corresponds to 2σ in the $\log T_{\rm eff}$) error to each side of the dots. Right: first input $SFR(t)$, dashed line. Also shown are the derived $SFR(t)$'s after 2, 4, 6, 8 and 10 iterations of the inversion method, dotted curves. The 12th iteration is given by the solid curve, showing convergence and a reliable recovery of the input $SFR(t)$.

where we further assume that the "observational" errors are well understood i.e. $\sigma(L)$ is known. Since the colour of a star having a given luminosity can sometimes be a multi-valued function, in practice we check along a given isochrone, to find all possible masses a given observed star might have as a function of time, and add all contributions (mostly 1, sometimes 2 and occasionally 3) in the same $G_i(t)$. Calculating this matrix is the only slow part of the procedure, and is equivalent to calculating the likelihood of one model. The likelihood

matrix $G_i(t)$ is the only input required by the method. The total number of stars is used as a normalization constraint at each iteration, needed to recover $SFR(t)$ from $Y(t)$. As mentioned earlier, it is not necessary to calculate the likelihood over the solution space being considered, i.e. $G_i(t)$ is only calculated once, which makes the method highly efficient.

Given the degeneracy of isochrones of different ages in the main sequence region, the lower fraction of the HR diagram is of relevance only in establishing the total normalization condition, and not in determining the shape of the $SFR(t)$. For this reason, we only include in the inference procedure stars with $\log L) > 0$, other stars are only used in fixing the overall normalization. The final results are not affected by this cut, but the iterative procedure converges much more rapidly and in a numerically more stable way if the lower degenerate and high error region of the HR diagram is excluded.

In Fig. 1 we also show the results of the first 12 iterations of the method every 2 iterations, which form a sequence of increasing resemblance to the input $SFR(t)$. The distance between successive iterations decreases monotonically at all ages, which together with the fact that after 12 iterations no further change is seen, shows the convergence of the method for this case. From the 2nd iteration (lowest dotted curve in the burst regions) it can be seen that the iteration of the variational calculus equation constructed from maximizing the likelihood is able to recover the input $SFR(t)$ efficiently. The positions, shapes and relative masses of the two bursts were correctly inferred by the 2nd iteration, although it took longer for the method to eliminate the populations outside of the two input bursts. The convergence solution is in remarkable agreement with the input $SFR(t)$, and only differs slightly, as seen from Fig. 1. No information was used in the inverting procedure beyond that which is available from the synthetic HR diagram, which was used extensively in constructing the likelihood matrix $G_i(t)$, which is the only input required by the inversion. The variational calculus method recovers a $SFR(t)$ for which the first variation of the likelihood vanishes, without assuming any *a priori* condition on the $SFR(t)$, beyond being a continuous twice differentiable function of time.

3.2. Testing temporal resolution

The second test uses an input $SFR(t)$ which differs from the previous one in that the bursts are of much shorter duration and larger

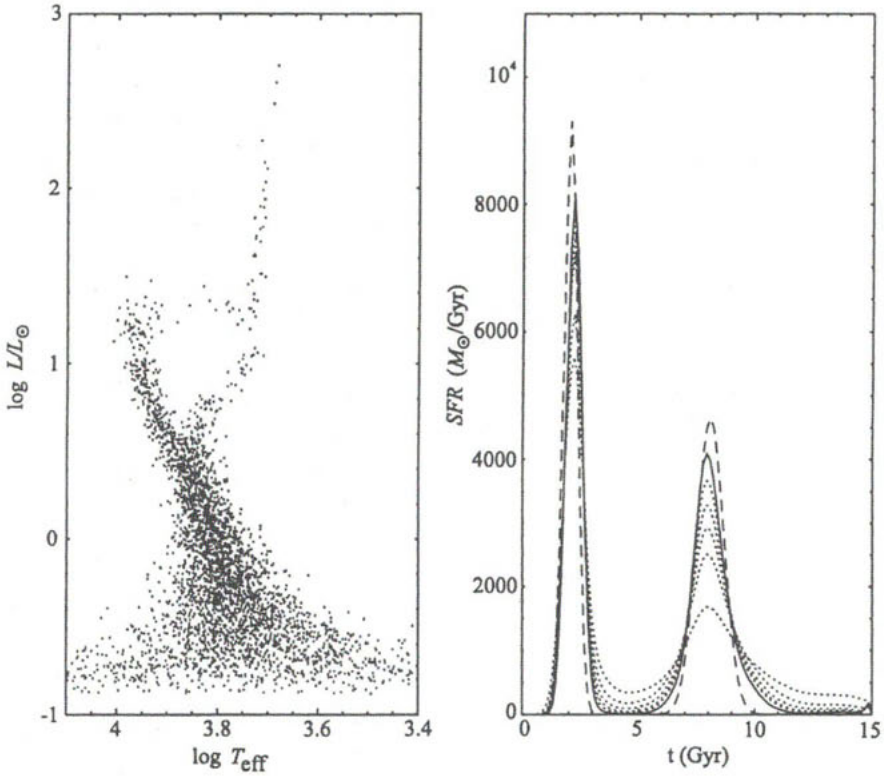

Fig. 2. Left: synthetic HR diagram resulting from the second input $SFR(t)$. Right: second input $SFR(t)$, dashed line. Also shown are the 3, 6, 9, 12 and 15 iterations of the inversion method, dotted curves. The 20th iteration is given by the solid curve, showing convergence and a reliable recovery of the input $SFR(t)$

amplitude, to approximately preserve the total number of stars. The input $SFR(t)$ of this case is shown by the dashed curve in the right panel of Fig. 2. The HR diagram which results from this $SFR(t)$ is shown in the left panel of Fig. 2 and shows basically the same populations as in Fig. 1 but with a much smaller spread, it contains a total of 3783 stars, with 1299 above $\log L) = 0$. The errors in these two cases were equal.

The inversion procedure is shown in the right panel of Fig. 2, were it can be seen that the convergence of the method remains ro-

bust, although this time it took slightly longer, the first 15 iterations are shown every 3. The $SFR(t)$ to which the method converged (after 20 iterations) again accurately reproduces the input one, the age, duration, amplitude and shape of the two input bursts were correctly inferred. That the shorter duration of the bursts was correctly inferred in this case shows that in the previous one the reconstructed age duration was not due to the spread caused by the errors, but was actually resolved in the data, and recovered correctly by the method. In this second case however, the spread due to the errors begins to be comparable to the intrinsic one of the input $SFR(t)$, and causes an artificial broadening of the recovered stellar ages, particularly in the older component. This last effect causes also a slight underestimate in the maximum amplitude of the bursts. Reducing the duration of the older component further would not produce a shorter duration in the inferred burst, unless the errors were also reduced.

That is, the method is capable of recovering the full age precision allowed by the observational errors.

3.3. Very old populations: sensitivity to photometric errors

The next test explores explicitly the way in which the method reacts to populations older than 10 Gyr, an approximate limit beyond which observational errors totally confuse the turn off points, in the adopted error distribution. A model $SFR(t)$ is shown by the dashed line in the right panel of Fig. 3. The left panel of Fig. 3 shows the resulting HR diagram which is used in the inversion process, and which only marginally differs from the one of Fig. 3.

Fig. 3 shows that the inversion procedure converged to a $SFR(t)$ which is a highly accurate representation of the input $SFR(t)$ in regions younger than around 10 Gyr. However, the star formation history for the oldest stars was not recovered.

Fig. 4 has the same input $SFR(t)$ as in case 3, and differs only in that a much lower noise level was assumed. In constructing the HR diagram seen in the left panel of Fig. 4 the numerical constant in Eq. (10) was reduced from 0.035 to 0.01. This lower noise level is reflected in the clearer HR diagram, where the older population is now distinguishable from the noise of the younger main sequence. The right panel in Fig. 4 shows the result of the inversion procedure, which differs from case 3 mostly in the speed with which the method converged, only 10 iterations were needed. The few stars in the oldest

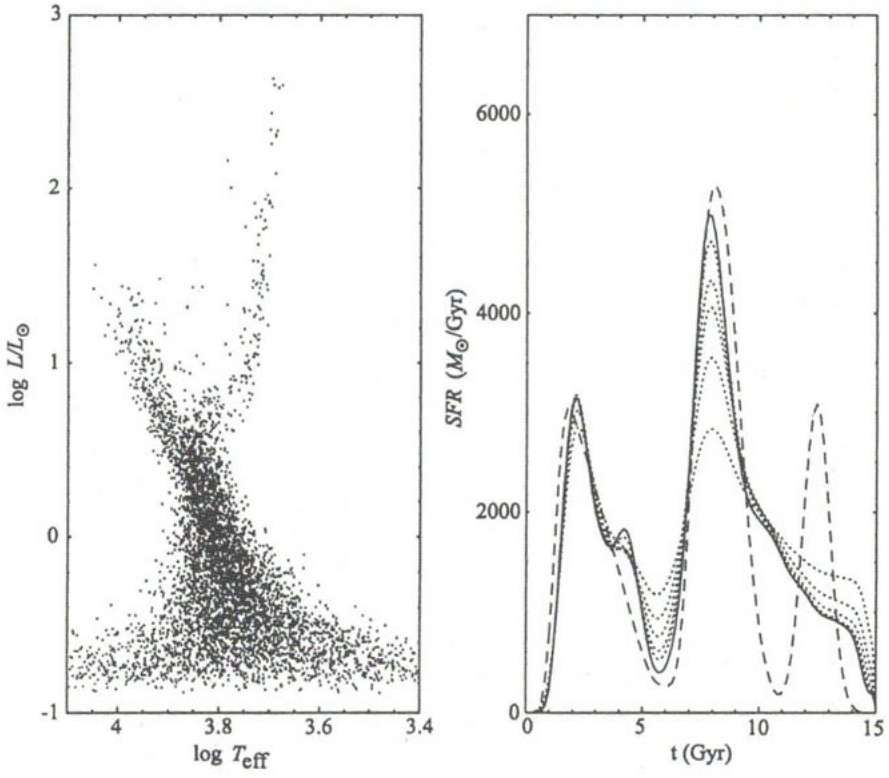

Fig. 3. Left: synthetic HR diagram resulting from the fifth input $SFR(t)$. Right: fifth input $SFR(t)$, dashed line. Also shown are the 3, 6, 9, 12 and 15 iterations of the inversion method, dotted curves. The 20th iteration is given by the solid curve, showing convergence and a good recovery of the input $SFR(t)$ for $t < 10$ Gyr.

component which can be separated from the younger main sequence are sufficient to accurately recover the shape for this burst.

In general, the variational calculus treatment of the maximum likelihood problem, together with the iterative method for solving the resulting equation, works well within the practical limits set by the "observational" errors. Having assumed only that the $SFR(t)$ was a continuous function of time, the method manages to recover the input function quite accurately, under conditions similar to those feasible for *Gaia* observations.

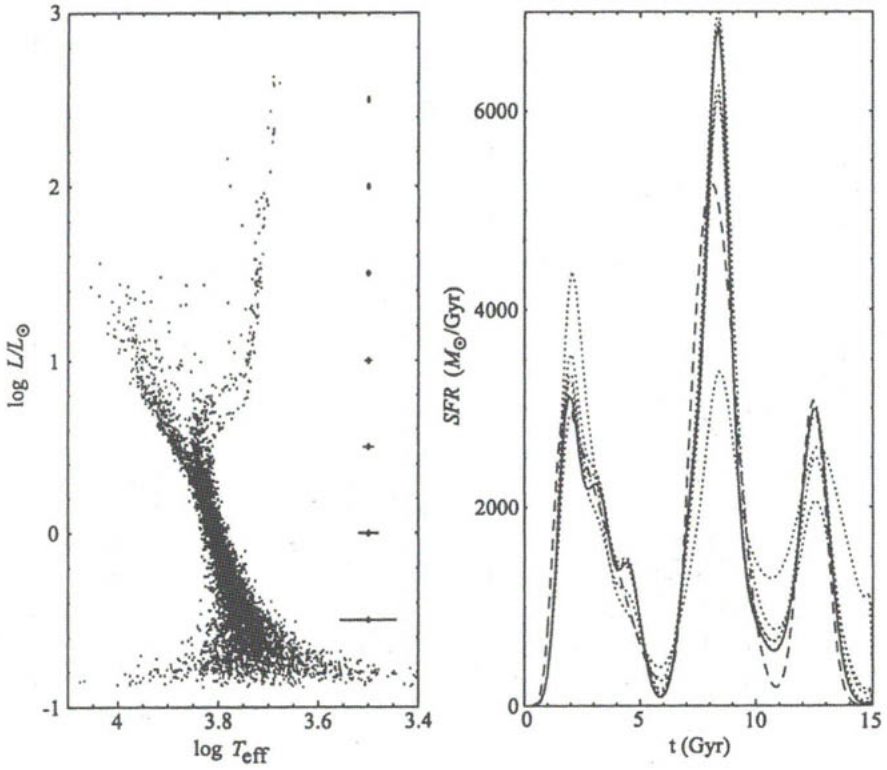

Fig. 4. Left: synthetic HR diagram resulting from the fifth input $SFR(t)$, produced using a much lower noise level. As in Fig. 1, the length of the bars to the right corresponds to 2σ in the $\log L$ error to each side of the dots. Right: fifth input $SFR(t)$, dashed line. Also shown are the 2, 4, 6, 8 and 9 iterations of the inversion method, dotted curves. The 10th iteration is given by the solid curve, showing rapid convergence and a good recovery of the input $SFR(t)$.

4. SENSITIVITY TO UNCERTAINTIES IN IMF, METALLICITY AND BINARIES

Uncertainties in the IMF, metallicity and binaries differ from simple sample size or photometric error in inducing a systematic mismatch between the isochrones used in any specific calculation and those which describe the astrophysics of the HR diagram being inverted. The following tests show the sensitivity of the method

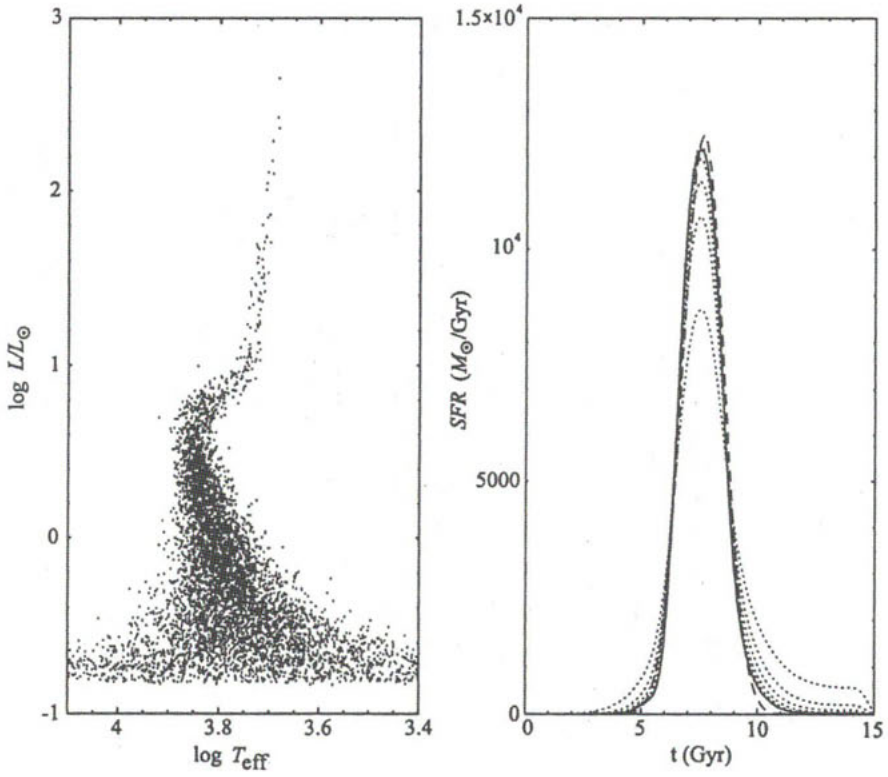

Fig. 5. Left: synthetic HR diagram resulting from the control input $SFR(t)$. Right: sixth input $SFR(t)$, dashed line. Also shown are the 3, 6, 9, 12 and 15 iterations of the inversion method, dotted curves. The 18th iteration is given by the solid curve, showing convergence and an accurate recovery of the input $SFR(t)$. This is used as a control case against which to compare variations in the assumed IMF, metallicity and binary fraction.

to uncertainties in the input IMF, metallicities and binary fraction. Firstly we present Fig. 5, the synthetic HR diagram contains 6340 stars with 1808 brighter than $\log L = 0$, and the input $SFR(t)$ is shown by the dashed line in the right panel of Fig. 5. The inversion of this HR diagram clearly shows again the convergence of the method to an accurate representation of the input $SFR(t)$. This test was included to define a control case to which variations can be compared.

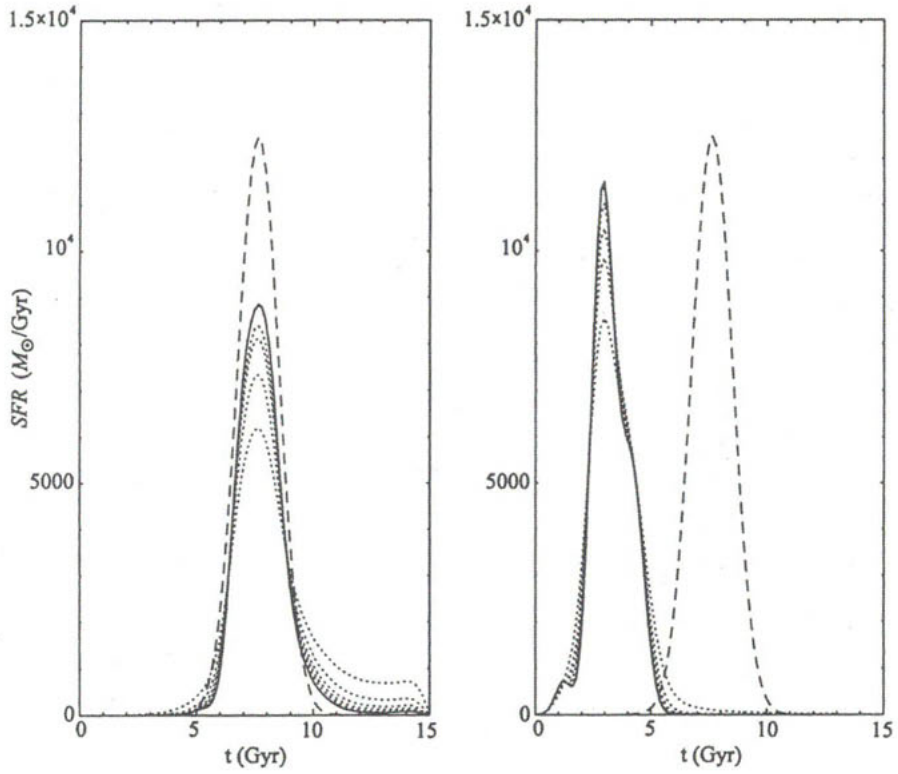

Fig. 6. Left: sixth input $SFR(t)$, dashed line. Also shown are the 3, 6, 9, 12 and 15 iterations of the inversion method, dotted curves. The 18 iteration is given by the solid curve, assuming an IMF much more weighted towards smaller masses than the one used for the HR diagram, which produces a normalization error. Right: sixth input $SFR(t)$, dashed line. Also shown are the 3, 6, 9, 12 and 15 iterations of the inversion method, dotted curves. The 18th iteration is given by the solid curve, assuming a metallicity one order of magnitude higher than the one used for the HR diagram, which results in the method converging to a younger $SFR(t)$.

4.1. IMF mismatch

The left panel in Fig. 6 shows the results of applying the inversion procedure with a "wrong" IMF to the HR diagram in Fig. 5 which was produced using the IMF of Eq. (9). The inversion procedure

assumed an IMF $\rho(m) \propto m^{-3}$ for all masses. Comparing Fig. 5 and the left panel in Fig. 6 it can be seen that the main effect of an error in the IMF is a distorted normalization, which is based on the total number of stars. The IMF used in the inversion is one in which low mass stars are more dominant than in the IMF used to construct the HR diagram, as a result, a lower $SFR(t)$ sufficed to produce the correct number of stars. As the colour and luminosity of a star of a given age and mass are not affected by changes in the IMF, the location of the relevant populations was not affected. The net result of changing the IMF used in the inversion was a reduction of the recovered $SFR(t)$ by a factor of 0.85, which is the factor by which the mass in stars in the mass region which we are sampling differs between the two IMF's. The convergence of the method was similarly unaffected. We can conclude that errors in the IMF used, within the expected uncertainties, do not affect the temporal structure of the derived star formation history significantly, but do affect its normalization. This quantifies the case for precise knowledge of the *Gaia* selection function.

4.2. Metallicity mismatch

In the following tests we investigate the effects of an uncertainty in the metallicity; the well known degeneracy between the inferred age and metallicity of an observed stellar population will be evident. Fig. 6, right panel shows the result of inverting the HR diagram of Fig. 5, which was produced using a metallicity of $[Fe/H] = -1.7$, using this time isochrones for $[Fe/H] = -0.7$ in the inversion procedure. The convergence of the method was not affected, and proceeded at the same rate as in the previous two cases, as the same HR diagram was used. The result of having assumed a metallicity one order of magnitude higher than that of the stellar population being inverted is a $SFR(t)$ much younger than the input one, as can be seen from Fig. 6, right panel. This discrepancy is due to the fact that the isochrones used in the inversion have very different temperatures and luminosities for stars of a given mass, from those of the isochrones used to generate the HR diagram. Actually, the colours and luminosities of stars from the higher metallicity isochrones approximately correspond to those of younger stars from the lower metallicity isochrones, the age-metallicity degeneracy. Having used isochrones in the inversion procedure which do not correspond to the stars being studied also confuses the method and the shape of the

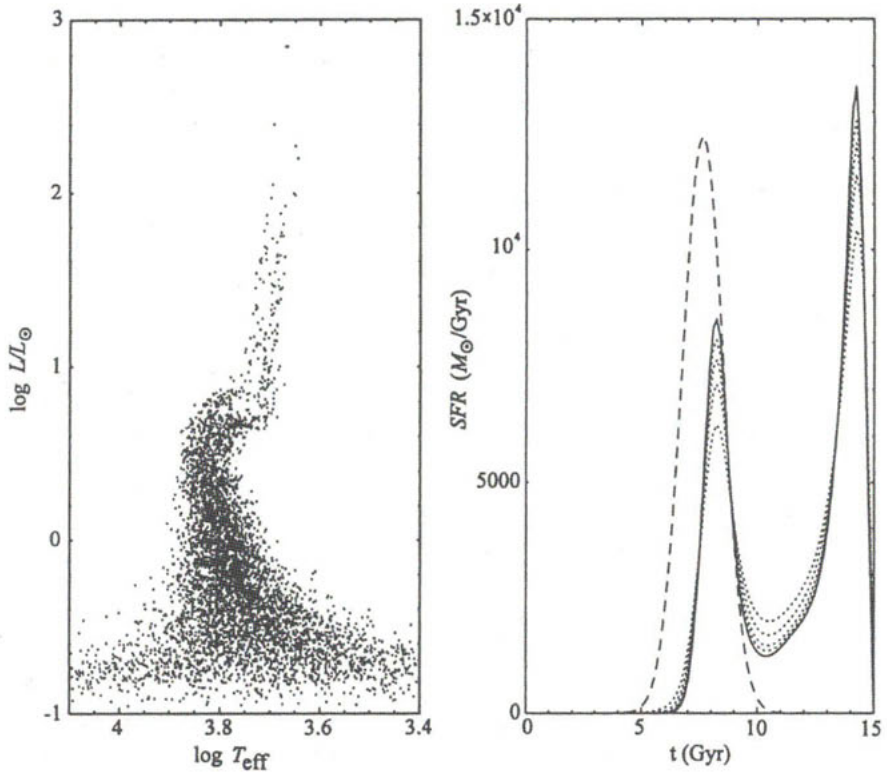

Fig. 7. Left: synthetic HR diagram resulting from the sixth input $SFR(t)$, produced using a metallicity of $[Fe/H]_\odot = -1.7$ for the stars older than 7.5 Gyr and of $[Fe/H]_\odot = -0.7$ for the stars younger than 7.5 Gyr. Right: sixth input $SFR(t)$, dashed line. Also shown are the 3, 6, 9, 12 and 15 iterations of the inversion method, dotted curves. The 18th iteration is given by the solid curve, assuming a constant metallicity for the entire evolution, which confuses the method.

recovered $SFR(t)$ is slightly distorted. The younger age assigned to the stars being analyzed also produces a slightly lower total $SFR(t)$, as with a younger population a larger fraction of the stars live into the present day HR diagram.

We also consider the complementary test, where the HR diagram is produced using a range of metallicities, and inverted assuming a single metallicity. This is presented in Fig. 7.

Fig. 7 shows the HR diagram which results from the input $SFR(t)$ of Fig. 5, with the difference that on this occasion the metallicity was not a delta function. In this case we used a metallicity of $[Fe/H] = -1.7$ for the stars older than 7.5 Gyr, and of $[Fe/H] = -0.7$ for the stars younger than 7.5 Gyr, i.e., a crude enrichment history. This is clearly seen in Fig. 7, where the two populations having different metallicities are evident, from the width of the RGB. As in all previous cases, the noise level was not changed. The result of applying the inversion method assuming a single metallicity of $[Fe/H] = -1.7$ is shown in the right panel of Fig. 7. The method correctly identifies the half of the $SFR(t)$ with the lower metallicity; the higher metallicity population is totally misinterpreted. Actually, the age the inversion procedure should assign to the high metallicity component is in fact greater than 15 Gyr, which is in contradiction with the fixed boundary condition of $SFR(15) = 0$. This makes the inversion procedure somewhat unstable, which in principle can be used to indicate that the isochrones being used in the inversion procedure do not correspond to the studied stars. The two distinct giant branches seen in this HR diagram indicate a difference in the metallicities of both populations.

As it might have been expected, uncertainties in the metallicity distort the inference procedure significantly, making determination of star formation histories robust only in cases where individual metallicities are available.

4.3. Binaries mismatch: optical and physical

As a final variation we consider the effects a non-zero unrecognized binary fraction would produce, which is shown in Fig. 8. It shows the HR diagram which results from the $SFR(t)$ of the previous tests, with the same IMF and metallicity of Fig. 5, but with the inclusion of a binary fraction of 0.5. Half of the stars generated had a secondary companion picked from the same IMF. The luminosity of the resulting binary is given by the sum of the luminosities of the two components, and its combined effective temperature through the Stefan-Boltzmann law. In the current observations of dSph galaxies and other similarly crowded fields the main contribution to the "binary" population comes not from physical binaries, but from observational confusion. Attempting to model this effect we picked the secondary star from the same IMF as the primary one (e.g. see Kroupa et al. (1993) for a discussion of binary confusion in

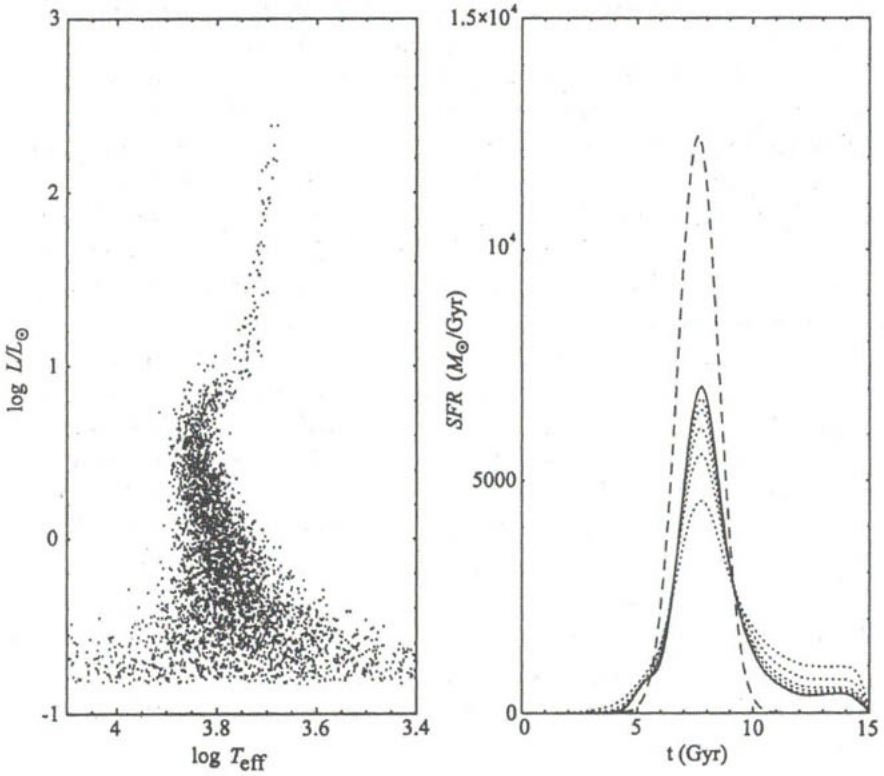

Fig. 8. Left: synthetic HR diagram resulting from the sixth input $SFR(t)$, produced using a binary fraction of 0.5. Right: sixth input $SFR(t)$, dashed line. Also shown are the 3, 6, 9, 12 and 15 iterations of the inversion method, dotted curves. The 18th iteration is given by the solid curve, assuming a binary fraction of 0, which results in a normalization error. The slight broadening of the MS is interpreted by the method as a small older component.

observations). We took the value of 0.5 for the binary fraction as a representative number from Kroupa et al. (1993).

As can be seen from comparing Figs. 8 and 5, the main result of having included a large unresolved binary fraction is a reduction in the total number of stars; the morphology of the HR diagram was not significantly affected. This last effect is due to the fact that the offset between the single star and the binary star main sequences is comparable to the noise in that region, producing only a slightly

broadened main sequence. The effects of binaries in other parts of the diagram are negligible, as the addition of a main sequence star to a giant does not affect the observed properties of the giant, and the odds of getting a binary giant are slim. The results of the inversion method are shown in the right panel of Fig. 8, where the dashed line shows the input $SFR(t)$, and the dotted and solid curves the first 18 iterations of the method, every 3. The convergence of the method is not affected, and proceeds quite rapidly. It can be seen that the method accurately identifies the age, duration and structure of the input burst, although with a normalization error which results from the reduction in the total number of stars seen. A further slight discrepancy between the input $SFR(t)$ and the recovered one appears at old ages, as the method confuses the broadening in the main sequence for a minor, extended age population. As with the errors in the IMF, having neglected the effects of binaries affects mostly the normalization of the recovered $SFR(t)$, distorting the general shape only slightly.

5. CONCLUSIONS CONCERNING THE METHOD

We can summarize our methodological results as follows:

(1) We have introduced a variational calculus scheme for solving maximum likelihood problems, and tested it successfully in the particular case of inverting HR diagrams.

(2) Assuming a known IMF and metallicity we have presented a non-parametric method for inverting HR diagrams which yields good results when recovering stellar populations younger than 10 Gyr, with data quality similar to those attained in current HST observations of dSph galaxies. Populations older than 10 Gyr can only be recovered equally well from HR diagrams with much reduced observational errors.

(3) Uncertainties in the IMF and binary fractions result in normalization errors on the total $SFR(t)$. Given the existence of an age-metallicity degeneracy on the colours and magnitudes of stars, an error in the assumed metallicity results in a seriously mistaken $SFR(t)$. This makes the version of the variational calculus approach we present here useful only in cases where the metallicity of the stars is knowable independently of the form of the colour-magnitude diagram near the turnoff.

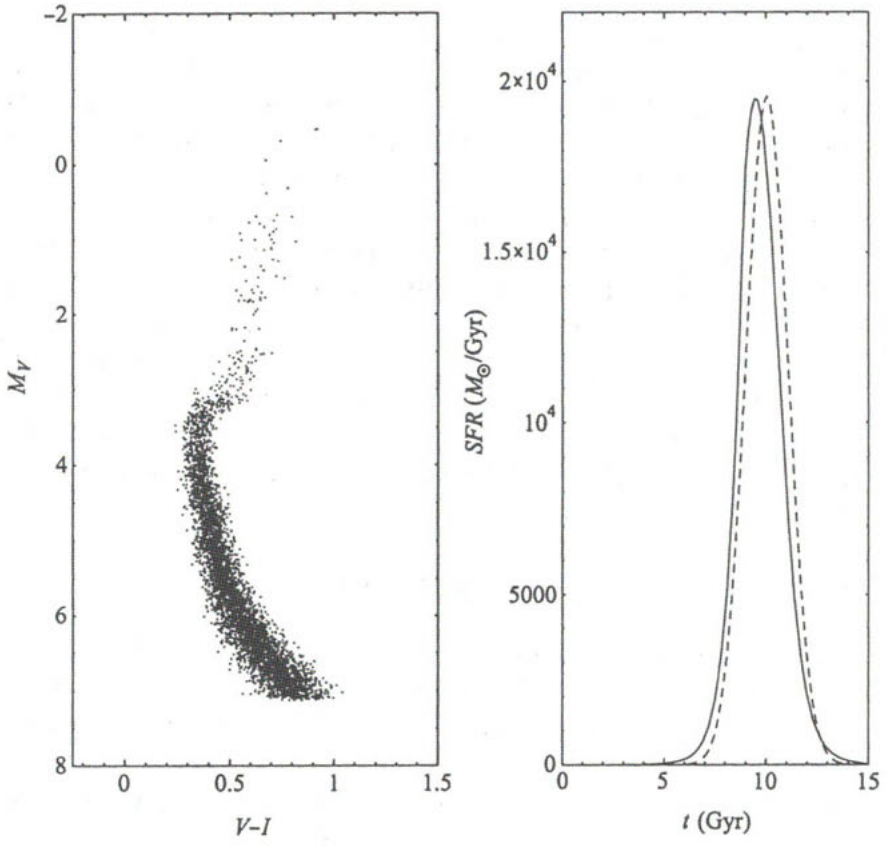

Fig. 9. Left: synthetic HR diagram for an "old" component, using isochrones of $[Fe/H] = -1.5$, and including a 10 % observational error. Right: inferred $SFR(t)$ for the "old" component, assuming the correct metallicity of $[Fe/H] = -1.5$, solid curve. The dotted curve shows the input $SFR(t)$. Comparison of the two curves shows the accuracy to which the age structure of an old population could be recovered using current statistical methods, if data having errors of $\leq$10 % in luminosity and temperature, and comparable in metallicity, were available.

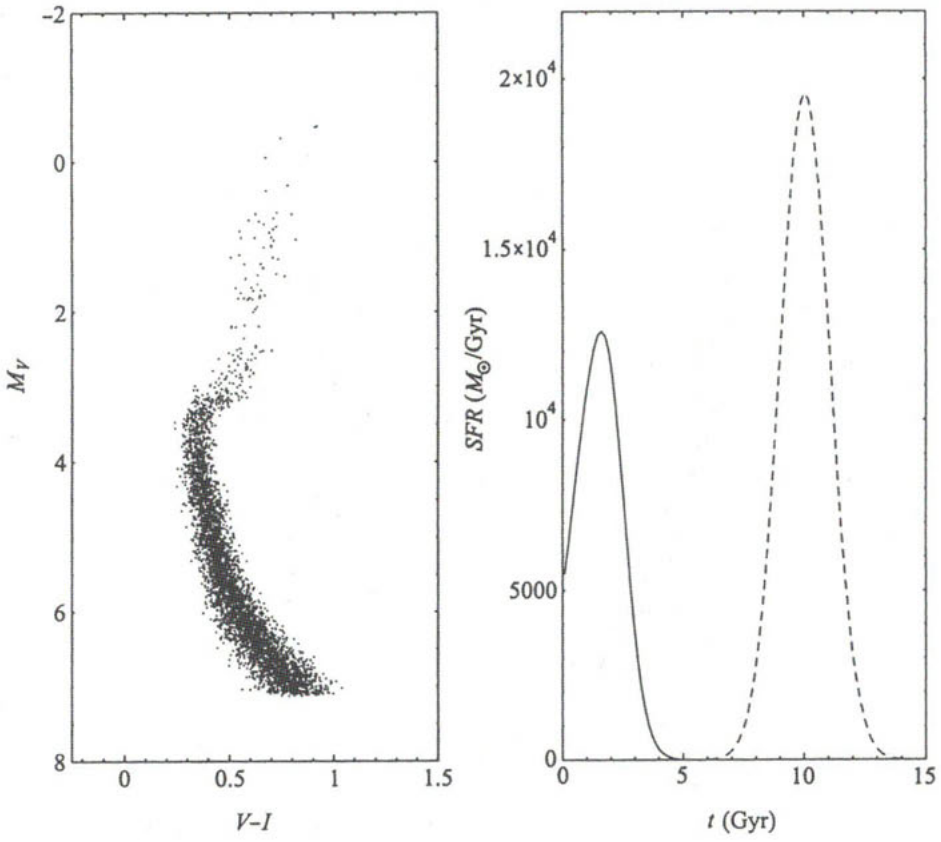

Fig. 10. Left: same HR diagram as in Fig. 9. Right: inferred $SFR(t)$ for the "old" component, assuming a metallicity of $[Fe/H] = 0$, solid curve. The dotted curve shows the input $SFR(t)$. Comparing these two curves shows the extent of the age-metallicity degeneracy in this case. Thus, unless metallicities are available, gross analysis errors are inevitable.

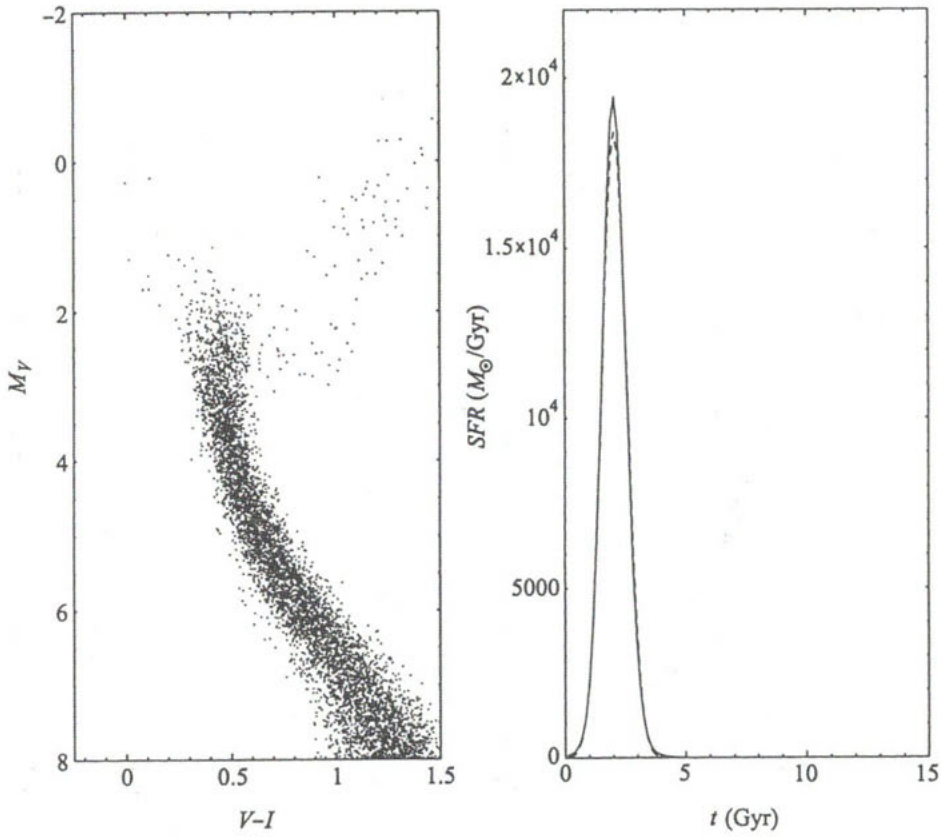

Fig. 11. Left: synthetic HR diagram for an "arm" component, using isochrones of solar metallicity, and including a 10 % observational error. Right: inferred $SFR(t)$ for the "arm" component, assuming the correct metallicity of $[Fe/H] = 0.0$, solid curve. The dotted curve shows the input $SFR(t)$. Comparison of the two curves shows the accuracy to which the age structure of a young population could be recovered using current statistical methods, if data having errors of $\leq$10 % were available.

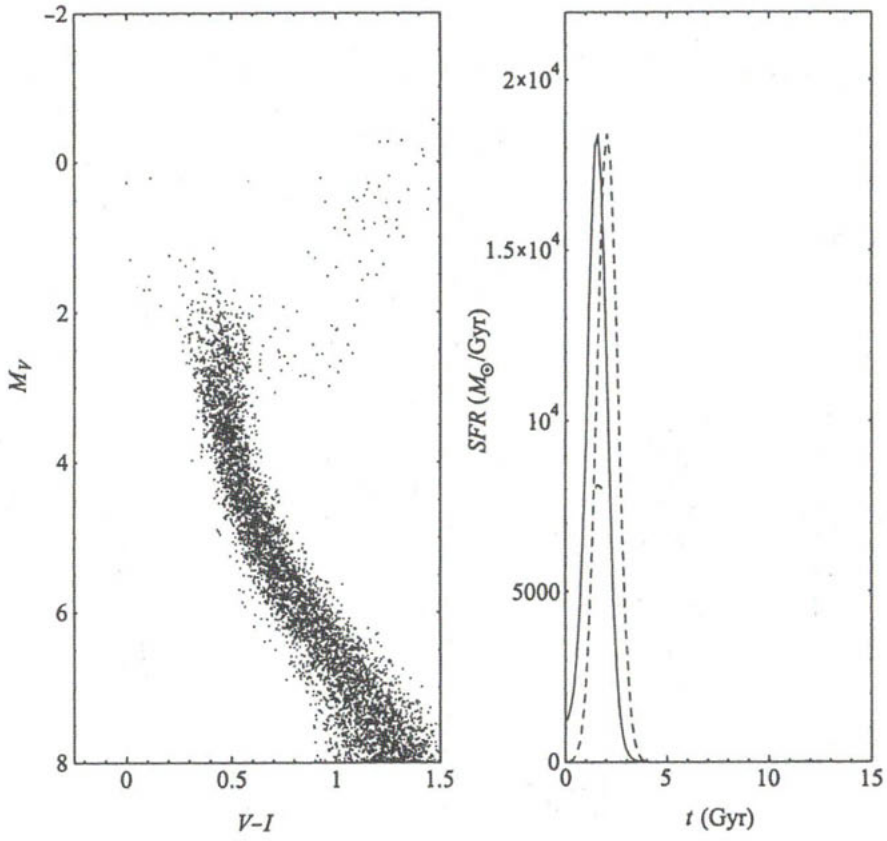

Fig. 12. Left: same HR diagram as in Fig. 11. Right: inferred $SFR(t)$ for the "arm" component, assuming a metallicity slightly off, of $[Fe/H] = 0.18$, solid curve. The dotted curve shows the input $SFR(t)$. Comparing these two curves shows the extent of the age-metallicity degeneracy in this case i.e. fine details in the build up history of the disk could be accurately recovered, if metallicities of the relevant populations were known to a ~ 0.2 dex accuracy.

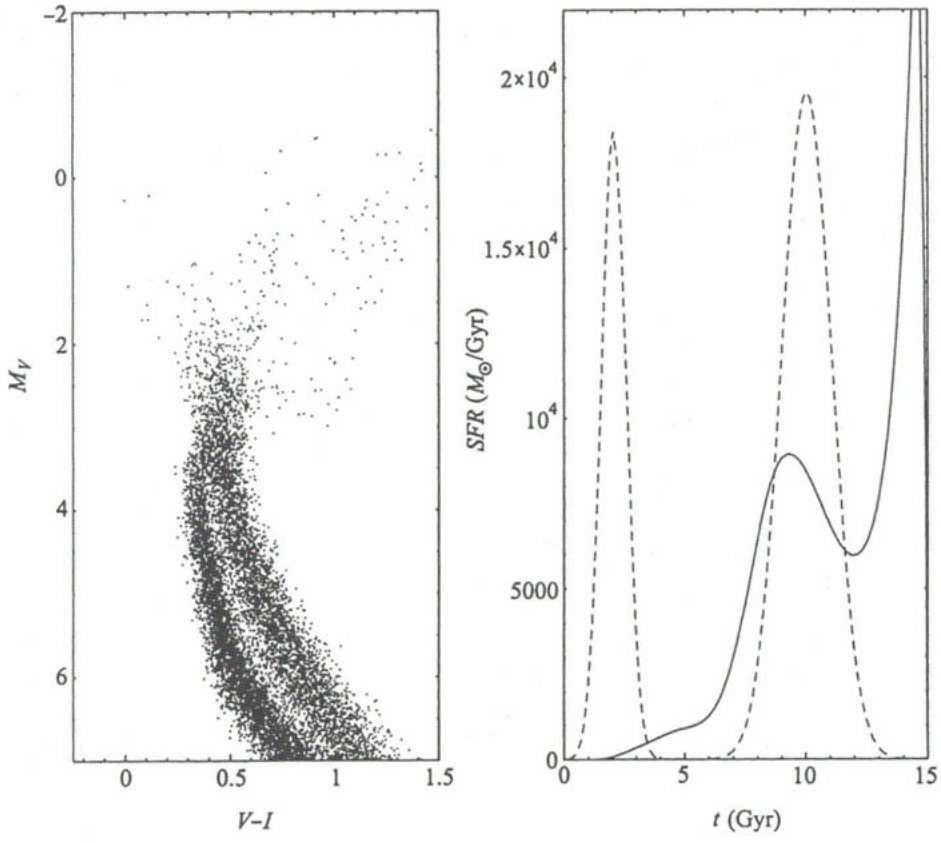

Fig. 13. Left: combined HR diagram including both components. Right: inferred $SFR(t)$ for the combined HR diagram, assuming a metallicity of $[Fe/H] = -1.5$, solid curve. The dotted curve shows the total $SFR(t)$ for these two components. Comparison of the two curves shows that useful information relative to galactic structure can only be obtained if the different populations present in an integrated HR diagram can be separated.

6. SIMULATIONS RELEVANT TO GAIA

The main-sequence turnoff of the oldest stellar populations corresponds to apparent magnitude ~ 20 at the galactic center, and near the apparent outer edge of the disk. *Gaia* can therefore determine the full star formation history of the near half of the Milky Way for all ages. This provides a sufficiently large sample that the global star formation history of our Galaxy can indeed be determined by *Gaia*. The star formation history at more recent times can also be determined for larger distances, especially in the Magellanic Clouds and Sgr dSph. Such determinations however require metallicity measures accurate to about 0.2 dex, and photometric data able to provide stellar effective temperatures good to about 10 % of $T_{\rm eff}$, for stars at and above the turnoff.

Figures 9–13 illustrate calculations specific to *Gaia* observations of stars at a distance of ~ 10 kpc.

7. CONCLUSIONS

The general implications for the *Gaia* mission include:

(1) The *Gaia* data set can be analysed to determine the star formation history of the Milky Way Galaxy, one of our primary science goals;
(2) This determination requires a well-known selection function from the central bulge to the outer galactic disk, at the *Gaia* limiting magnitude;
(3) Individual stellar metallicities are required for a large, well-defined, although not necessarily complete, sample of stars, with an accuracy ideally as good as 0.2 dex;
(4) Effective temperatures must be determinable for these same stars with an accuracy of about 10 %;
(5) This precision shares the final uncertainty equally between stellar temperature, stellar metallicity and distance uncertainty.

REFERENCES

Aparicio A., Bertelli G., Chiosi C., Garcia-Pelayo J. M. 1990, A&A, 240, 262

Aparicio A., Gallart C. 1995, AJ, 110, 2105

Aparicio A., Gallart C., Bertelli G. 1997, AJ, 114, 669
Chiosi C., Bertelli G., Meylan G., Ortolani S. 1989, A&A, 219, 167
Da Costa G.S. 1994, ESO/OHP Workshop on Dwarf Galaxies, eds. G. Meylan & P. Prugniel, p. 221
Dolphin A. 1997, New Astronomy, 2, 397
Fagotto F., Bressan A., Bertelli G., Chiosi C. 1994, A&AS, 104, 365
Girardi L., Bressan A., Chiosi C., Bertelli G., Nasi E. 1996, A&AS 117, 113
Grebel E.K. 1997, preprint, astro-ph 9706191
Hurley-Keller D., Mateo M., Nemec J. 1998, AJ, 115, 1840
Kroupa P., Tout C.A., Gilmore G. 1993, MNRAS, 262, 545
Mighell K.J., Butcher H.R. 1992, A&A, 255, 26
Mighell K.J. 1997, AJ, 114, 1458
Mould J.R., Han M., Stetson P.B., Gibson B., Graham J.A., Huchra J., Madore B., Rawson D. 1997, ApJ, 483, L41
Ng Y.K. 1998, A&AS, 132, 133
Smecker-Hane T.A., Stetson P.B., Hesser J.E., Lehnert M.D. 1994, AJ, 108, 507
Tolstoy E. 1995, PhD Thesis, Groeningen University, The Netherlands
Tolstoy E., Saha A. 1996, ApJ, 462, 672